# Loss Mechanisms in Dielectric-Loaded Resonators

KAWTHAR A. ZAKI, SENIOR MEMBER, IEEE, AND CHUNMING CHEN, STUDENT MEMBER, IEEE

*Abstract*—**Analysis is presented of resonators consisting of a section of a dielectric-loaded waveguide shorted at both ends. The analysis includes resonant frequency calculations, mode charts, and unloaded $Q$ computations. Numerical results are presented for the unloaded $Q$'s of various modes, as a function of the resonator parameters. Effects of losses in different parts of the resonator wall on the unloaded $Q$ are discussed, and methods of improving these $Q$'s are explored.**

**Experimental verification of the theoretically derived results is made for a number of resonators, and the measurements agree closely with theory.**

## I. Introduction

MANY APPLICATIONS require the availability of microwave resonators with low loss and small size. Dielectric-loaded waveguide resonators are suitable for such applications as highly temperature stable oscillators [1], [2], low-noise microwave synthesizers [3], and bandpass filters [4]–[6]. This paper presents properties of resonators consisting of a section of a dielectric-loaded waveguide shorted at both ends with particular emphasis on the (ohmic) loss mechanisms that affect their unloaded $Q$'s. Previous analysis has considered losses only due to radiation from unshielded resonators [7]. Explicit closed-form analytical expressions for the unloaded $Q$'s are derived for the hybrid modes, with the contributions of the losses in each section of the resonator's boundary separately identified. Numerical results are presented for different modes.

A number of dielectric-loaded resonators were constructed, and their resonant frequencies and unloaded $Q$'s were accurately measured. The experimentally measured results are presented, and are found to agree closely with the theoretical calculations.

## II. Resonator Geometry, Resonant Frequency, and Mode Charts

The dielectric-loaded resonator geometry under consideration is shown in Fig. 1. It consists of a section of length $L$ of a perfectly conducting outer cylindrical waveguide of radius $b$, axially loaded with a concentric dielectric cylinder of radius $a$ and relative permittivity $\epsilon_{r_1}$. The region $a < r < b$ has relative permittivity $\epsilon_{r_2}$. The two ends of the resonator are perfectly conducting planes. Analysis of this type of resonator is very useful for the understanding of the more general case where the dielectric rod is shorter than the total cylinder length $L$.

Manuscript received March 15, 1985; revised May 25, 1985. This material is based upon work supported by the National Science Foundation under Grant ECS-832049.

The authors are with the Department of Electrical Engineering, University of Maryland, College Park, MD 20742.

The structure of Fig. 1 can resonate in various modes which correspond to the modes of propagation in the cylindrical loaded waveguide discussed in [8]. These modes can be axially symmetric (i.e., transverse electric $TE_{0mn}$ or transverse magnetic $TM_{0mn}$), or hybrid modes $HE_{lmn}$. The resonant frequency of any of these modes is computed from applying the boundary conditions that the tangential electric fields must vanish on the ends of the resonator. This condition yields

$$\sin \beta L = 0 \quad \beta L = n\pi, \qquad n = 1, 2, \cdots \tag{1}$$

where $\beta$ is the propagation constant of the mode in an infinite waveguide with the same cross section as the resonator ($\beta^2 = -\gamma^2$). Determination of the resonant frequency involves solving the characteristic equation (2) for the wave number $\xi_1$, (see [8] for details)

$$G_n(\xi_1 a) = U_n^2 a^2 \gamma^2 + k_0^2 a^2 V_n W_n = 0 \tag{2}$$

where

$$\xi_1^2 = k_1^2 + \gamma^2 \quad \zeta_2^2 = -\left(k_2^2 + \gamma^2\right)$$

$$k_1^2 = \epsilon_{r_1} k_0^2 \quad k_2^2 = \epsilon_{r_2} k_0^2 \quad k_0^2 = \omega^2 \mu_0 \epsilon_0$$

$$U_n = n J_n(\xi_1 a)\left[\frac{1}{\xi_1^2 a^2} + \frac{1}{\zeta_2^2 a^2}\right]$$

$$V_n = \left[\frac{J_n'(\xi_1 a)}{\xi_1 a} + \frac{P_n'(\zeta_2 a)}{\zeta_2 a}\right] \quad \alpha = \frac{-U_n}{V_n}$$

$$W_n = \left[\epsilon_{r_1}\frac{J_n'(\xi_1 a)}{\xi_i a} + \epsilon_{r_2}\frac{R_n(\zeta_2 a)}{\zeta_2 a}\right]$$

$$P_n(\zeta_2 r) = J_n(\xi_1 a)\left[\frac{K_n(\zeta_2 r) I_n'(\zeta_2 b) - I_n(\zeta_2 r) K_n'(\zeta_2 b)}{K_n(\zeta_2 a) I'(\zeta_2 b) - I_n(\zeta_2 a) K_n'(\zeta_2 b)}\right]$$

$$R_n(\zeta_2 r) = J_n(\xi_1 a)\left[\frac{K_n(\zeta_2 r) I_n(\zeta_2 b) - I_n(\zeta_2 r) K_n(\zeta_2 b)}{K_n(\zeta_2 a) I_n(\zeta_2 b) - I_n(\zeta_2 a) K_n(\zeta_2 b)}\right]$$

and where $J_n(\cdot)$, $I_n(\cdot)$, and $K_n(\cdot)$ are the Bessel functions and the modified Bessel functions of first and second kinds, respectively.

One of the most important considerations in the area of dielectric-loaded resonators is the ability to accurately predict the resonant frequencies of the modes that can exist within the resonator as a function of its parameters so that desired modes can be chosen and spurious modes may be avoided. For homogeneously filled waveguides, this is usu-

0018-9480/85/1200-1448$01.00 ©1985 IEEE

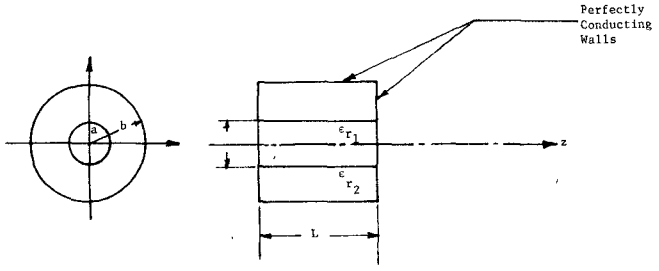


Fig. 1. Dielectric-loaded resonator consisting of a short-circuited section of a dielectric-loaded waveguide.

ally done using what is commonly known as the "mode charts." The mode charts for the homogeneously filled waveguides are plots of $(fD)^2$ versus $(D/L)^2$, where $D$ is the waveguide diameter, $f$ is the resonant frequency, and $L$ is the resonator length. The choice of these particular combinations of parameters is made since this choice leads to a simple linear relationship. For the case of the dielectric-loaded resonator, the situation is more complex since there are several additional parameters. However, an attempt to construct similar mode charts for dielectric-loaded resonators revealed some interesting similarities to the case of homogeneously filled resonators. Fig. 2 is a mode chart for a resonator with $a = 0.394''$, $b = 0.5''$, and $\epsilon_{r_1} = 37.6$. The figure is a plot of $(fD)^2$ versus $(D/L)^2$, where $D = 2a$ is the dielectric diameter. The plots are almost linear, except near small values of $(D/L)^2$, where significant deviation from linearity is apparent.

## III. Unloaded $Q$ Calculations

Determination of the resonators unloaded $Q$'s involves the calculation of the energy $(U)$ stored in the resonator and the power $(W_L)$ lost in the metallic walls and in the dielectric. The unloaded $Q$ is then calculated from the definition

$$Q = \frac{\omega_0 U}{W_L} \tag{3}$$

where $\omega_0$ is the resonant angular frequency.

Although the calculation of the $Q$ is conceptually simple, the details are rather involved. In the following, closed-form expressions are given of the relevant quantities.

First, the energy stored $U$ is computed as the sum of the stored energies both inside the dielectric $\epsilon_{r_1}(U_1)$ and in the region between the dielectric and the conducting waveguide walls $(U_2)$. Thus

$$U = U_1 + U_2 \tag{4}$$

where

$$U_1 = \frac{\epsilon_1}{2}\int_0^a\int_0^{2\pi}\int_0^L \bar{E}\cdot\bar{E}^* r\,dr\,d\phi\,dz$$

$$U_2 = \frac{\epsilon_2}{2}\int_a^b\int_0^{2\pi}\int_0^L \bar{E}\cdot\bar{E}^* r\,dr\,d\phi\,dz$$

$\bar{E}$ is the field in the resonator given in [8]. The integrals can be calculated in a closed form, and the results are listed in

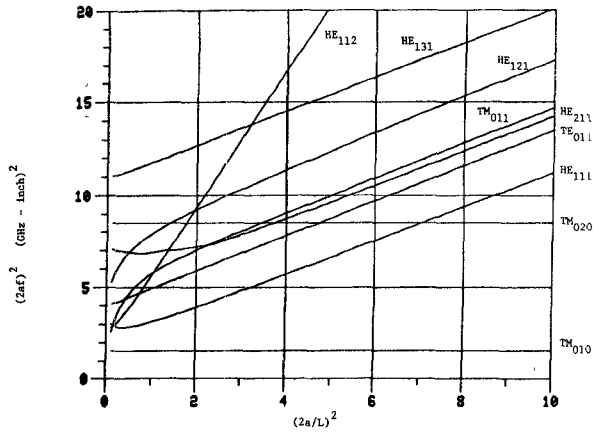


Fig. 2. Mode chart of dielectric-loaded resonator. $a = 0.394$ in, $b = 1.2a$, $\epsilon_{r_1} = 37.6$, $\epsilon_{r_2} = 1.0$.

(5) and (6)

$$U_1 = \frac{\pi L \epsilon_0 \epsilon_{r_1}}{4} \cdot \Bigg[ J_n^2(\xi_1 a)\left\{\frac{a^2}{2}\left(1-\frac{n^2}{\xi_1^2 a^2}\right)\cdot\left(1+\beta^2\frac{1+\alpha^2}{\xi_1^2}\right)+\frac{2\beta^2 n\alpha}{\xi_1^4}\right\} + J_n'^2(\xi_1 a)\left\{\frac{a^2}{2}\left(1+\beta^2\frac{1+\alpha^2}{\xi_1^2}\right)\right\} + J_n(\xi_1 a)J_n'(\xi_1 a)a\beta^2\frac{1+\alpha^2}{\xi_1^3}\Bigg] \tag{5}$$

$$U_2 = \frac{\pi L \epsilon_0 \epsilon_{r_2}}{4} \cdot \Bigg[ -P_n^2(\zeta_2 b)\frac{b^2}{2}\frac{\beta^2\alpha^2}{\zeta_2^2}\left(1+\frac{n^2}{\zeta_2^2 b^2}\right) + R_n'^2(\zeta_2 b)\frac{b^2}{2}\left(\frac{\beta^2}{\zeta_2^2}-1\right) - J_n^2(\xi_1 a)\left\{\frac{a^2}{2}\left(1+\frac{n^2}{\zeta_2^2 a^2}\right)\left(1-\beta^2\frac{1+\alpha^2}{\zeta_2^2}\right)+\frac{2\beta^2 n\alpha}{\zeta_2^4}\right\} + R_n'^2(\zeta_2 a)\frac{a^2}{2}\left\{1-\frac{\beta^2}{\zeta_2^2}\right\} - P_n'^2(\zeta_2 a)\frac{a^2\alpha^2}{2}\cdot\frac{\beta^2}{\zeta_2^2} - J_n(\xi_1 a)\frac{\beta^2 a}{\zeta_2^3}\{R_n'(\zeta_2 a)+\alpha^2 P_n'(\zeta_2 a)\}\Bigg]. \tag{6}$$

The power lost in the resonator walls and in the dielectric are computed based on the low-loss assumptions, that the fields are unperturbed by the losses. The surface current density in the conducting walls is determined from the tangential magnetic fields. The dielectric loss is the product of the stored energy in the dielectric and the loss tangent. Accordingly, the dielectric loss is merely proportional to $U_1$ given in (5), while the conductor loss $W_c$ is expressed as

$$W_c = W_s + 2W_B \tag{7}$$

where $W_s$ is the loss in the side walls (or circumference) of the resonator and $W_B$ is the loss in each of the ends (base and top). $W_B$ is further separated as

$$W_B = W_{B_1} + W_{B_2} \tag{8}$$

where $W_{B_1}$ is the loss in the base region $0 < r < a$ covered by the dielectric ($\epsilon_{r_1}$), and $W_{B_2}$ is the loss in the annular base region $a < r < b$ under the dielectric ($\epsilon_{r_2}$). These losses are evaluated from the integrals

$$W_S = \frac{R_s}{2}\int_0^{2\pi}\int_0^{L}\left(H_\phi H_\phi^* + H_z H_z^*\right) b\, d\phi\, dz$$

$$W_{B1} = \frac{R_s}{2}\int_0^{2\pi}\int_0^{a}\left(H_r H_r^* + H_\phi H_\phi^*\right) r\, dr\, d\phi$$

$$W_{B2} = \frac{R_s}{2}\int_0^{2\pi}\int_a^{b}\left(H_r H_r^* + H_\phi H_\phi^*\right) r\, dr\, d\phi$$

where $R_S$ is the conductor's surface resistance, $H_r$, $H_\phi$, and $H_z$ are the magnetic field components in the resonator given in [8]. Closed-from expressions for the above integrals are given in the following:

$$W_s = \frac{\pi b L R_s}{4}\left[\frac{\alpha^2\beta^2}{\omega^2\mu^2}P^2(\zeta_2 b) + \frac{1}{\zeta_2^4}\left\{\omega\epsilon_2\zeta_2 R_n'(\zeta_2 b) + \frac{\alpha\beta^2 n}{\omega\mu b}P_n(\zeta_2 b)\right\}^2\right] \tag{9}$$

$$W_{B1} = \frac{\pi R_s}{2\xi_1^4}\cdot\left[\left\{\frac{\xi_1^2 a^2}{2}\left(1-\frac{n^2}{\xi_1^2 a^2}\right)\left(\omega^2\epsilon_1^2 + \frac{\alpha^2\beta^4}{\omega^2\mu^2}\right) + \frac{2\alpha\beta^2\epsilon_1 n}{\mu}\right\}J_n^2(\xi_1 a) + \frac{\xi^2 a^2}{2}\left\{\omega^2\epsilon_1^2 + \frac{\alpha^2\beta^4}{\omega^2\mu^2}\right\}J_n'(\xi_1 a) + \xi_1 a\left\{\omega^2\epsilon_1^2 + \frac{\alpha^2\beta^4}{\omega^2\mu^2}\right\}J_n(\xi_1 a)J_n'(\xi_1 a)\right] \tag{10}$$

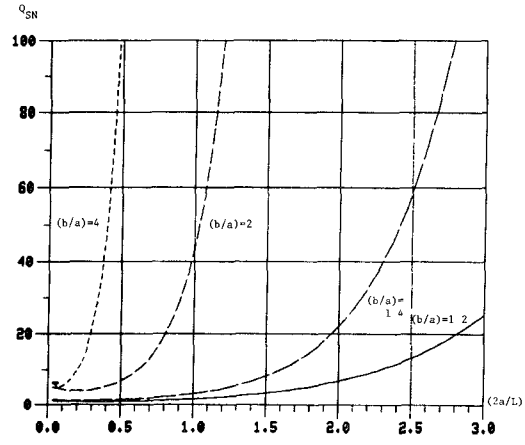


Fig. 3. $Q_{SN}$ for $HE_{111}$ mode versus $(2a/L)$.

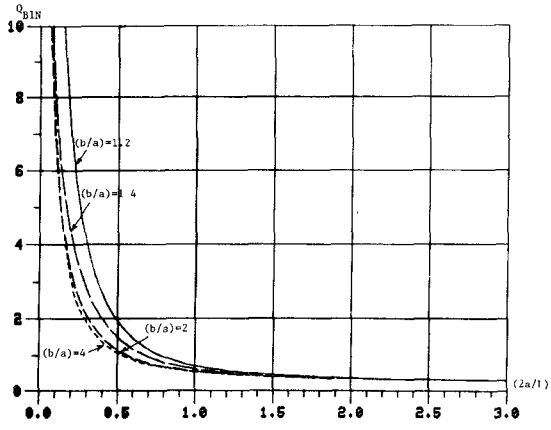


Fig. 4. $Q_{B1N}$ for $HE_{111}$ mode versus $(2a/L)$.

$$W_{B2} = \frac{\pi R_s}{2\zeta_2^4}\cdot\left[\frac{-b^2\zeta_2^2}{2}\left(1+\frac{n^2}{\zeta_2^2 b^2}\right)\frac{\alpha^2\beta^4}{\omega^2\mu^2}P_n^2(\zeta_2 b) + \frac{b^2\zeta_2^2}{2}\omega^2\epsilon_2^2 R_n'^2(\zeta_2 b) + \left\{\frac{a^2\zeta_2^2}{2}\left(1+\frac{n^2}{\zeta_2^2 a^2}\right)\left(\omega^2\epsilon_2^2 + \frac{\alpha^2\beta^4}{\omega^2\mu^2}\right) - \frac{2\alpha\beta^2\epsilon_2 n}{\mu}\right\}J_n^2(\xi_1 a) - \frac{a^2\zeta_2^2}{2}\left\{\omega^2\epsilon_2^2 R_n'^2(\zeta_2 a) + \frac{\alpha^2\beta^4}{\omega^2\mu^2}P_n'^2(\zeta_2 a)\right\} - \zeta_2 a\left\{\omega^2\epsilon_2^2 R_n'(\zeta_2 a) + \frac{\alpha^2\beta^4}{\omega^2\mu^2}P_n'(\zeta_2 a)\right\}J_n(\xi_1 a)\right]. \tag{11}$$

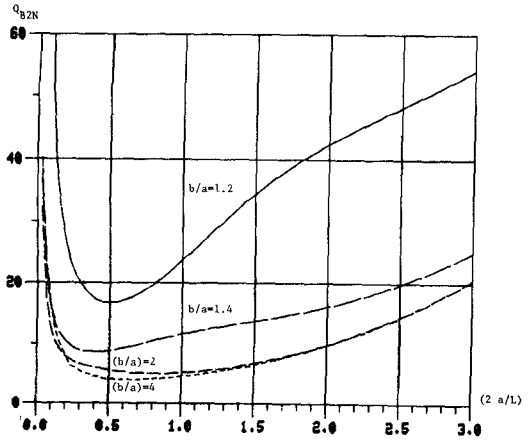


Fig. 5. $Q_{B2N}$ for $HE_{111}$ mode versus $(2a/L)$.

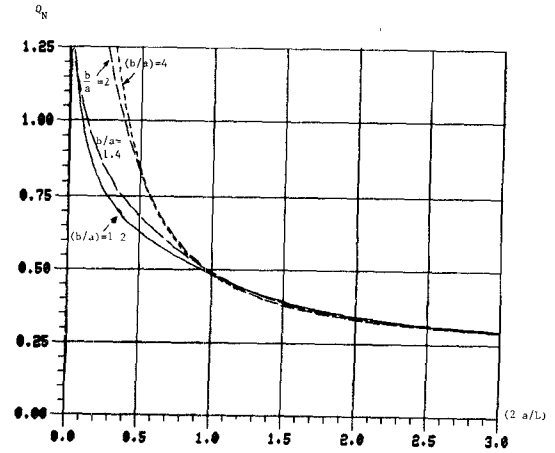


Fig. 7. Unloaded $Q_N$ for $HE_{111}$ mode versus $(2a/L)$.

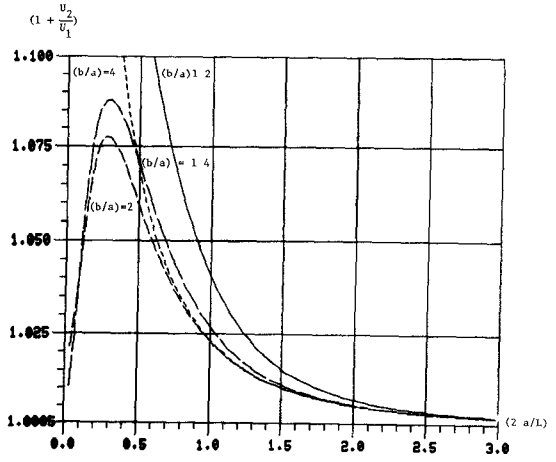


Fig. 6. Variation of $Q_D \tan\delta$ with $(2a/L)$ for $HE_{111}$ mode.

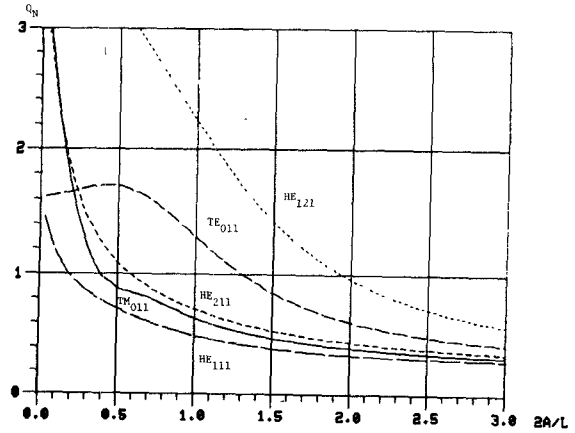


Fig. 8. $Q_N$ for different modes versus, $(2a/L)$.

## IV. Numerical and Experimental Results

To ascertain the effects of the losses in the various parts of the resonator, it is convenient to express the total unloaded $Q$ in terms of the factors $Q_S$, $Q_{B1}$, $Q_{B2}$, and $Q_D$ corresponding to the losses $W_S$, $W_{B1}$, $W_{B2}$, and $W_D$, respectively, where $W_D$ is the loss in the dielectric

$$\frac{1}{Q}=\frac{1}{Q_S}+\frac{1}{Q_{B1}}+\frac{1}{Q_{B2}}+\frac{1}{Q_D}. \tag{12}$$

Variations of each of these $Q$'s (normalized by $(\delta/\lambda)$, where $\delta$ is the skin depth and $\lambda$ is the wavelength in the dielectric medium $\epsilon_{r_1}$ at resonance), with $(2a/L)$ and $(b/a)$ as parameters are shown in Figs. 3–6 for the $HE_{111}$ mode. For $(b/a)>1.4$, the loss $W_S$ becomes negligibly small. Fig. 6 shows that for the cases analyzed ($\epsilon_{r_1} \gg \epsilon_{r_2}$), $Q_D$ will always be approximately equal to $1/\tan\delta$ (here $\delta$ is the loss tangent of $\epsilon_{r_1}$). Variation of the total normalized unloaded $Q$ (due to conductor loss only) with $(2a/L)$ is shown in Fig. 7.

Fig. 8 shows the total normalized unloaded $Q$ due to the conductor loss only for the first few hybrid modes.

To experimentally verify the analysis, several dielectric-loaded cavities were constructed and their resonant frequencies and unloaded $Q$'s were measured. The dielectric constant of the material used in the resonator was first measured accurately using the technique described in [9]. To eliminate the inaccuracy due to the variation of the dielectric constant from sample to sample, the same dielectric sample was used in cavities of equal lengths but different diameters. The dielectric sample was supported within each cavity by means of an annular piece of very low-loss foam material ($\epsilon_r=1.02$). The resonators were coupled very lightly to coaxial lines by means of probes extending slightly into the cavitites at their middle. These probes couple to the radial electric fields of the $HE_{111}$ mode. The resonant frequency and unloaded $Q$'s were measured by the amplitude reflection method [10]. Extra care had to be taken to ensure that the dielectric resonators ends had tight contact with both the end planes of the metallic cavity. Both the resonant frequency and unloaded $Q$'s were extremely sensitive to this contact.

Fig. 9 is a sample measured result of the resonant frequency variation with the ratio $(b/a)$. In this figure, the theoretical curve (shown by the solid line) has a maximum deviation of 0.23 percent from the measured data.

The unloaded $Q$'s of the same resonators were also measured, and the comparison with the calculated values is shown in Table I.

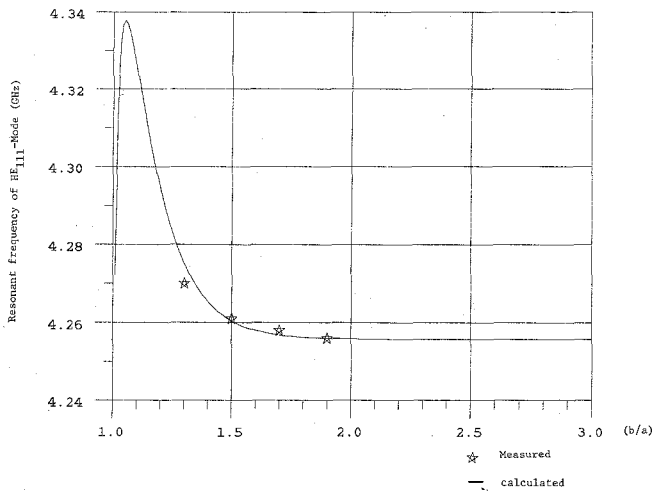


Fig. 9. Calculated and measured resonant frequency of an $HE_{111}$-mode dielectric-loaded resonator. $a = 0.3436$ in, $\epsilon_{r_1} = 29.45$, $L = 0.3002$ in.

TABLE I
CALCULATED AND MEASURED RESULTS OF THE UNLOADED $Q$'S

| $(\frac{b}{a})$ | Measured $Q_u$ | Calculated$^{(*)}Q_u$ | % |
|---|---|---|---|
| 1.3 | 4071 | 3287 | -19.3% |
| 1.5 | 3258 | 3262 | 0.12% |
| 1.7 | 3992 | 3254 | -18.5% |
| 1.9 | 3488 | 3250 | -6.8% |

(*) Based on Aluminum conductivity of $3.72 \times 10^7$ mhos/meter.

## V. Discussion and Conclusion

Examination of Figs. 3–5, and 7 shows that for $(2a/L) > 1$, the loss $W_{B1}$ dominates the other conductor losses $W_{B2}$ and $W_S$. Therefore, qualitatively, to minimize the losses $W_{B1}$, the resonator should be constructed so that the conducting end walls are not contacting the dielectric. The fields outside the dielectric would decay rapidly in the axial direction, greatly reducing the current density (and, hence, the losses) on the end walls. This, however, would perturb the modal fields in the resonator; the resonant frequencies and unloaded $Q$'s will not be as simple to compute as in the present case. The measured unloaded $Q$'s given in Table I are almost always larger than the theoretical values. This perhaps is due to the imperfect contact between the dielectric and the conducting ends of the cavity, which tends to reduce the losses $W_{B1}$ in the base and top regions.

When all the conducting walls are far enough from the dielectric, the conductor losses will be negligible with respect to the dielectric loss, and, therefore, the unloaded $Q$ in this case will be equal to approximately $1/\tan\delta$, regardless of the mode.

The closed-form analytical expressions for the energy stored and the losses in dielectric-loaded resonators presented in this paper allowed the determination of the quantitative distribution of these parameters.

## References

[1] H. Abe *et al.* "A highly stabilized low noise GaAs FET integrated oscillator with a dielectric resonator in the *C*-band," *IEEE Trans. Microwave Theory Tech.*, vol. MTT-26, pp. 156–163, March 1978.

[2] S. Tatsuguchi *et al.*, "An integrated 18 GHz receiver front end using a dielectric resonator stabilized generator," in *ICC-79, Conf. Rec.* vol. 1, pp. 262.1–262.5.

[3] G. D. Alley and H. C. Wang, "An ultra low-noise microwave synthesizer," in *1979 IEEE Int. Microwave Symp. Dig.*, pp. 147–149.

[4] J. K. Plourde and D. F. Linn, "Microwave dielectric resonator filters using $Ba_2Ti_2O_{20}$ Ceramics," *IEEE Trans. Microwave Theory Tech.*, vol. MTT-27, pp. 233–238, Mar. 1979.

[5] A. E. Atia and R. R. Bonetti, "Generalized dielectric resonator filters," *COMSAT Tech. Rev.*, vol. 11, no. 2, pp. 321–343, Fall 1981.

[6] S. J. Fiedziusko, "Dual-mode dielectric resonator loaded cavity filters," *IEEE Trans. Microwave Theory Tech.*, vol. MTT-30, pp. 1311–1316, Sept. 1982.

[7] Y. Kobayashi and S. Tanaka, "Resonant modes of a dielectric rod resonator short circuited at both ends by parallel conducting plates," *IEEE Trans. Microwave Theory Tech.*, vol. MTT-28, pp. 1077–1085, Oct. 1980.

[8] K. A. Zaki and A. E. Atia, "Modes in dielectric-loaded waveguides and resonators," *IEEE Trans. Microwave Theory Tech.*, vol. MTT-31, pp. 1039–1045, Dec. 1983.

[9] W. E. Courtney, "Analysis and evaluation of a method of measuring the complex permittivity of microwave insulators," *IEEE Trans. Microwave Theory Tech.*, vol. MTT-18, pp. 476–485, Aug. 1970.

[10] D. Kajfez and E. J. Hwan, "*Q*-factor measurement with network analyzer," *IEEE Trans. Microwave Theory Tech.*, vol. MTT-32, pp. 666–670, July 1984.

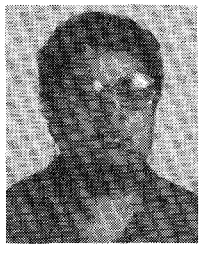

**Kawthar A. Zaki** (SM'85) received the B.S. degree with honors from Ain Shams University, Cairo, Egypt, in 1962, and the M.S. and Ph.D. degrees from the University of California, Berkeley, in 1966 and 1969, respectively, all in electrical engineering.

From 1962 to 1964, she was a Lecturer in the Department of Electrical Engineering, Ain Shams University. From 1965 to 1969, she held the position of Research Assistant in the Electronic Research Laboratory, University of California, Berkeley. She joined the Electrical Engineering Department, University of Maryland, College Park, MD, in 1970, where she is presently an Associate Professor. Her research interests are in the areas of electromagnetics, microwave circuits, optimization, and computer-aided design.

Dr. Zaki is a member of Tau Beta Pi.

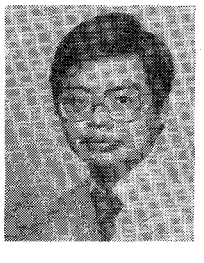

**Chunming Chen** (S'85) was born in Taiwan, Republic of China, in 1958. He received the B.S. degree from the National Tsing Hua University, Taiwan, in 1981, and the M.S. degree from the University of Maryland, College Park, in 1985, both in electrical engineering.

Since 1984, he has worked as a Research Assistant in the Department of Electrical Engineering, University of Maryland, College Park. He is now working towards a Ph.D. degree in the area of microwave components and circuits.